15.2 FLOW AND DRAG MECHANISMS RESULTING FROM THE INTERACTION OF GRAVITY WAVES WITH A TURBULENT BOUNDARY LAYER.

Maria Athanassiadou *and Andrew R. Brown
Met Office, Bracknell, Berkshire U.K.

1. INTRODUCTION

The problem of air flow over complex terrain is traditionally approached from two somewhat distinct directions, depending primarily on the scale of the orography involved. On one side, the boundary layer view usually considers neutrally stratified turbulent flows over small hills embedded within the boundary layer, with extensions to moderately stable stratified flow. On the other hand, a larger scale point of view of the orography, examines stably stratified flow over hills or mountains that penetrate the boundary layer. In the latter case, the effects of the boundary layer are either assumed negligible or enter through friction at the lower boundary without explicit consideration of the interaction. Neglecting non-linear effects, the Froude number $F_{ra} = U/Na$, based on the horizontal scale of the orography a, describes the transition from evanescent disturbances to propagating gravity waves, Figure 1. U is the flow velocity and N the Brunt Väisälä frequency.

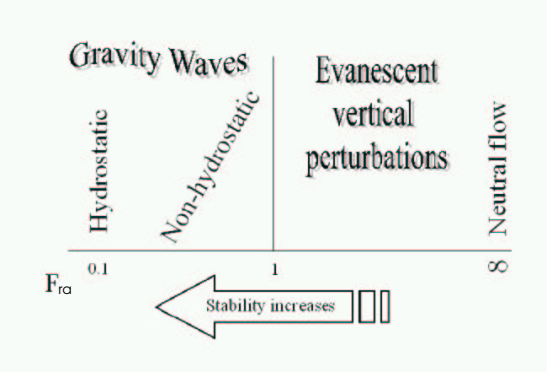

Figure 1: Schematic diagram of flow regimes, categorised by $F_{ra} = U/Na$.

The work examines both the behaviour of the flow near the surface as well as the general structure of the gravity waves. The emphasis is placed on the momentum balance and the various drag mechanisms due to gravity waves and turbulence, that coexist in this case. In particular, we want to understand relations of surface pressure drag, momentum flux above the boundary layer and distribution of the total drag within the boundary layer.

*Corresponding author address: Maria Athanassiadou, Met Office, Bracknell, Berkshire, RG12 2SZ, U.K.; email: maria.athanassiadou@metoffice.com

2. MODEL AND SIMULATIONS

The problem is examined numerically using the Met Office research model BLASIUS, a terrain following, non-linear, non-hydrostatic model that can be used as an inviscid model or with a choice of either a mixing length closure or a one-and-a half order turbulence scheme that carries the turbulent kinetic energy as a prognostic variable, Belcher and Wood (1996). We examine 2D hills, with a profile given by $z_s(x) = h/(1 + x^2/a^2)$. Orography of various a and maximum height h is employed, resulting in hills embedded in the boundary layer to hills of similar height to the boundary layer height z_i. The boundary layer is near neutral closer to the surface and capped by an inversion at z_i. Typical wind and normalised temperature (buoyancy), profiles of the approaching flow are shown in Figure 2.

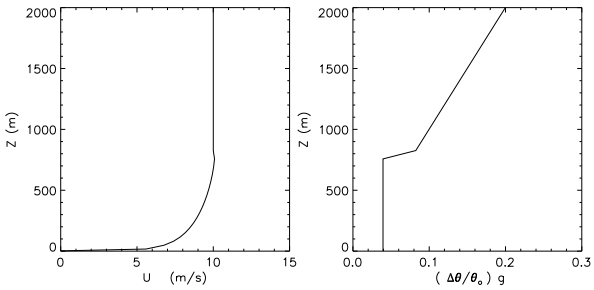

Figure 2: Typical profiles of the mean flow wind and normalised temperature.

3. RESULTS

Aspects of the flow are discussed first. Figure 3 shows the difference $\hat{w} = w(invisc) - w(bl)$, in the vertical velocity between a simulation with the

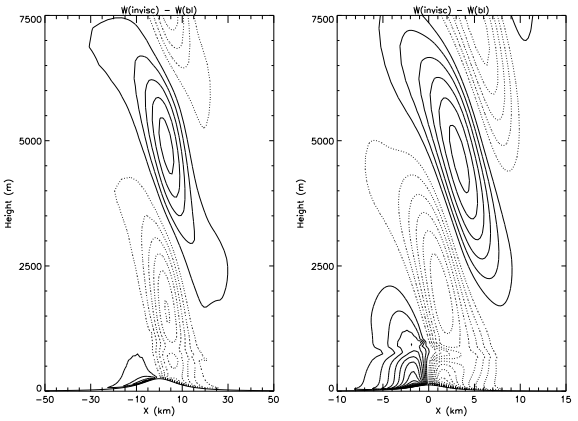

Figure 3: Difference in vertical velocity between an inviscid run and a run with a boundary layer. Left, for $F_{ra} = 0.1$; right, $F_{ra} = 0.4$. Contour interval, 0.01 m/s.

boundary layer and the equivalent inviscid one i.e., a simulation with the turbulence switched off and constant U, N and equal to the free stream values of the boundary layer simulation. The two cases shown are representative of a hydrostatic wave (left figure) and a non-hydrostatic wave (right figure). For all hydrostatic wave cases examined, the wave amplitude reduction, in the boundary layer simulation compared with the equivalent inviscid one, was about 20%. This difference was similar both above the boundary layer and inside it. For non-hydrostatic waves, the maximum reduction, $> 20\%$, occurs inside the boundary layer, with less reduction, $< 20\%$, above it. For larger Froude numbers, $\hat{w}$ in the boundary layer, resembles the inviscid evanescent solution, with equal magnitudes of negative and positive values, symmetry across the hill and the maximum near the surface. The boundary layer depth is about 760 m, as can be seen from Figure 2.

Figure 4 shows the surface pressure distribution for a hydrostatic wave case, $F_{ra} = 0.1$ and for a non-hydrostatic wave case, $F_{ra} = 0.4$. The dot-line is the inviscid solution. The solid line is from the boundary layer simulation. In both cases, the effect of the boundary layer is to reduce the amplitude as well as the phase shift relative to the hill, of the surface pressure perturbation. These results agree with Weng *et al.* 1997, although the basic flow here is somewhat different. Both the amplitude and phase shift of the surface pressure perturbation are more pronounced for the hydrostatic regime than the non-hydrostatic one. This, and in particular the larger phase shift of the surface pressure perturbation for small Froude numbers, is consistent with the larger difference of the drag coefficient between the boundary layer and inviscid solution observed for small F_{ra}, which is discussed later.

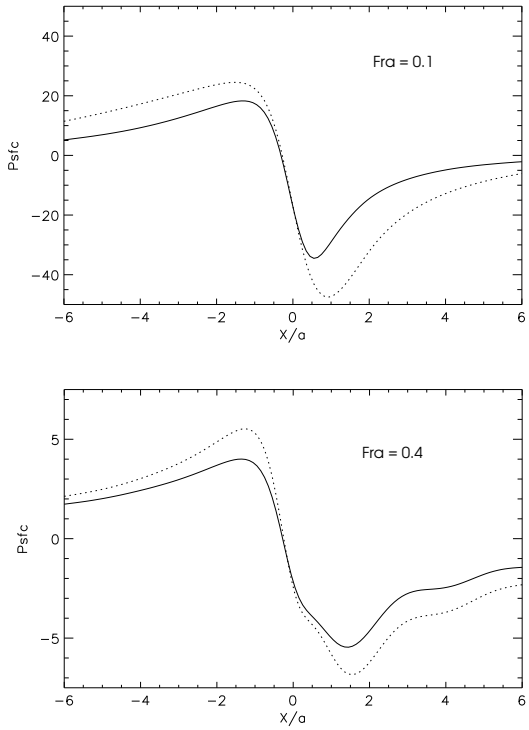

Figure 4: Surface pressure from an inviscid run (dot-line) and the equivalent run with a boundary layer (solid line). Cases for $F_{ra} = 0.1$ and $F_{ra} = 0.4$. Crest of the hill at $x = 0$.

Aspects of momentum balance and drag mechanisms are discussed next. For the type of flow and orography we consider here i.e., no flow separation, gentle hills with horizontal dimensions up to 10 km and therefore no Coriolis effects, the surface force can be decomposed in the following way:

$$F_{tot} = F_\tau + F_{pr} = F_\tau + F_p + F_w \qquad (1)$$

$F_\tau = \rho_s u_{*o}^2 + \Delta F_\tau \simeq \rho_s u_{*o}^2$, is the total frictional drag and has, in principle, two components. The first, $\rho_s u_{*o}^2$, is due to the friction stress over flat terrain before the hill and relates to the type of vegetation or other surface coverage. The second is a contribution from the stress perturbations, assumed small in practice. F_{pr} is the contribution to the total surface force due to surface pressure perturbations whose integral over the hill does not become zero. These can arise due to different mechanisms and hence result in different types of drag, thought

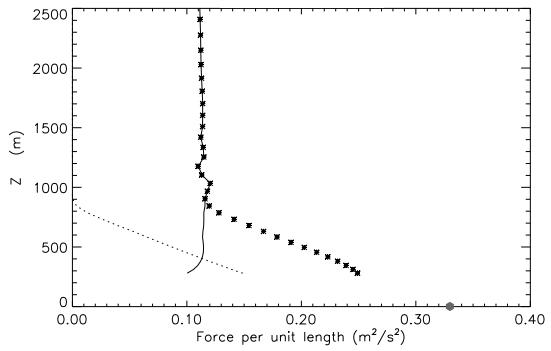

Figure 5: Vertical profiles of horizontally averaged shear stress (dot line), momentum flux by the waves (solid line) and their sum (stars). The symbol at the x-axis shows the total force on the surface.

not always independent of one another. Here, F_{pr} is decomposed into a wave drag F_w, relating to the gravity waves and a form drag F_p due to turbulence. For inviscid flow, $F_{pr} = F_w$. On the other hand, $F_{pr} = F_p$ for neutral or weakly stratified flow when $F_{ra} > 1$ and the flow cannot support gravity waves. For turbulent flow with gravity waves, both mechanisms are present. Their relative importance, relation and dependence on various parameters are some of the thins of interest in this work.

Figure 5, shows profiles of the horizontally averaged frictional stress, the momentum flux of the waves and their sum for a $F_{ra} = 0.2$ case. The frictional drag has its maximum value at the surface and it decreases to zero at the top of the boundary layer, z_i. Above the boundary layer, the total force is equal to the momentum flux of the gravity waves, $mf = \overline{-u'w'}$. The over-bar here denotes horizontal domain average. Inside the boundary layer, the total flux at each level, F_z, is equal to $\overline{\tau_{13}} + \overline{-u'w'}$, where $\overline{\tau_{13}}$ is the unresolved turbulent flow part. The vertical profile of F_z, extrapolates to F_{tot} at the surface and becomes just $\overline{-u'w'}$ above z_i. The momentum flux is almost constant within the boundary layer and similar to the value for $z > z_i$. The figure is qualitatively typical of most cases. The main difference between cases is the relative magnitudes of $\overline{-u'w'}$ and $\overline{\tau_{13}}$, depending on the dimensions of the hill.

Figure 6, shows the surface drag coefficient

$$W_c = \frac{F_{pr}}{U^2 h^2 / a} \qquad (2)$$

as a function of F_{ra}. The symbols are for boundary layer simulations and incorporate cases of different z_i/h and z_i/a. The solid line is the inviscid solution. Percentages represent the ratios between the boundary layer and inviscid solutions, for typical F_{ra} numbers. The results show a dependency only on stratification. The difference between the turbulent and inviscid solution is maximum in the hydrostatic wave regime and decreases with increasing F_{ra}.

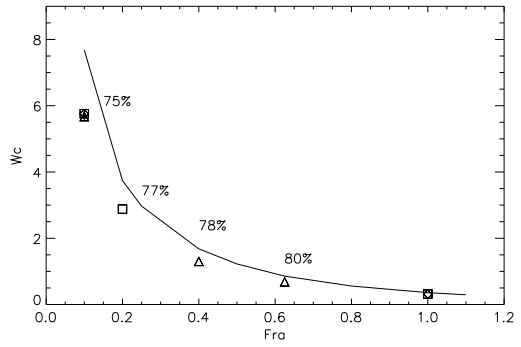

Figure 6: Drag coefficient as a function of stability. $\diamond$ for runs with $z_i/h = 1.5$; $\square$ for $z_i/h = 3$;$\triangle$ for $z_i/h = 6$, 7.6 and 9.5; $+$ for $z_i/h = 15$. The solid curve is the inviscid solution with constant U and N with height. The numbers indicate the percentage of the pressure drag coefficient from the inviscid linear solution.

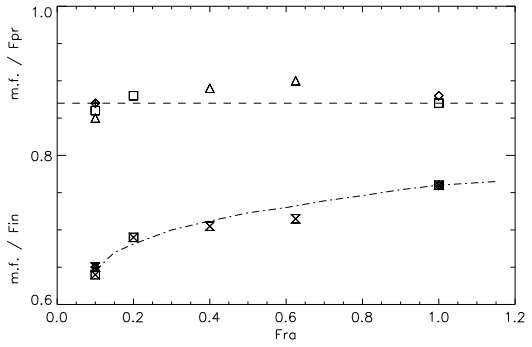

Figure 7: Normalised momentum flux as a function of stability. Symbols on top, mf/F_{pr}; lower symbols, mf/F_{in}.

Figure 7, shows the ratios of gravity wave momentum flux to total surface pressure force mf/F_{pr} (symbols around the dash line) and momentum flux to the surface pressure force from the inviscid solution mf/F_{in}, (symbols around the dash-dot line). The ratio $mf/F_pr \sim 0.87$ and is almost constant with F_{ra}. Moreover, no evidence of a dependence of mf/F_pr on z_i/h was found since the former was sim-

ilar for all hills considered and for all stratifications. On the other hand, mf/F_{in} increases with increasing F_{ra}. This shows a dependency of mf/F_{in} on z_i/a, since as we move towards larger Froude numbers, a is decreasing whereas z_i is the same in all simulations here.

4. SUMMARY

In this work, we try to 'merge' the two scale dependent views of orographic flows by considering gravity wave flow coexisting with a turbulent boundary layer. Aspects of the flow and aspects of momentum balance and drag mechanisms are considered.

The structure of the gravity waves inside the boundary layer is examined for various hill sizes. Apart from the amplitude reduction above the boundary layer, the wave solution differs from the inviscid one inside the boundary layer, the difference depending on F_{ra}.

The surface pressure perturbation in the case of boundary layer flow, shows a reduced amplitude and phase shift relative to the hill compared to inviscid flow. The phase shift is larger for waves in the hydrostatic regime and less for non-hydrostatic waves, or less stable stratification. This is consistent with the larger difference in the drag coefficient between the boundary layer and inviscid solution observed for small F_{ra}, compared with the smaller difference for larger F_{ra}.

The momentum flux of the gravity waves is constant inside the boundary layer despite the sheared flow there. No dependence was found, of the ratio of the gravity waves momentum flux to the surface pressure drag, on z_i/h, or F_{ra}.

The combined effects of gravity waves and turbulent boundary layer need to be properly represented in NWP models, that currently tend to treat these processes separately. This work aims to contribute towards this goal.

References

Belcher S. E. and N.Wood, 1996: Form and wave drag due to stably stratified turbulent flow over ridges, *Q.J.R.Meteorol.Soc.* **122**,863–902

Weng, W., Chan, L., Taylor, P. A., and Xu, D., 1997: Modelling stably stratified boundary-layer flow over low hills, *Q.J.R.Meteorol.Soc.* **123**, 1841–1866